Inorganic Chemistry
Article

Inorg. Chem. **2010**, *49*, 8713–8723 **8713**
DOI: 10.1021/ic100935b

Diphenyl(1-naphthyl)phosphine Ancillary for Assembling of Red and Orange-Emitting Ir(III) Based Phosphors; Strategic Synthesis, Photophysics, and Organic Light-Emitting Diode Fabrication

Bo-Sian Du,[†] Chen-Huey Lin,[†] Yun Chi,*[,†] Jui-Yi Hung,[†] Min-Wen Chung,[‡] Tsung-Yi Lin,[‡] Gene-Hsiang Lee,[‡] Ken-Tsung Wong,[‡] Pi-Tai Chou,*[,‡] Wen-Yi Hung,*[,§] and Hao-Chih Chiu[§]

[†]*Department of Chemistry, National Tsing Hua University, Hsinchu 300, Taiwan,* [‡]*Department of Chemistry, National Taiwan University, Taipei 106, Taiwan, and* [§]*Institute of Optoelectronic Sciences, National Taiwan Ocean University, Keelung 202, Taiwan*

Received May 11, 2010

Treatment of a series of dinuclear Ir(III) complexes $[(fnazo)_2Ir(\mu\text{-}Cl]_2$, $[(fpiq)_2Ir(\mu\text{-}Cl]_2$, and $[(fppy)_2Ir(\mu\text{-}Cl]_2$ with diphenyl(1-naphthyl)phosphine (dpnH) in decalin at 100 °C afforded the simple adducts, *trans-N,N′*-[$(fnazo)_2$Ir(dpnH)Cl] (**1a**), *trans-N,N′*-[$(fpiq)_2$Ir(dpnH)Cl] (**1b**), and *trans-N,N′*-[$(fppy)_2$Ir(dpnH)Cl] (**1c**), for which the C^N cyclometalating reagents, that is, fnazoH, fpiqH and fppyH, stands for 4-(4-fluorophenyl)quinazoline, 1-(4-fluorophenyl)isoquinoline and 4-fluorophenylpyridine, respectively. Single crystal X-ray diffraction study on **1a** revealed existence of two *trans-N,N′* cyclometalates, with both chloride and dpnH donors located at the positions opposite to the phenyl substituents. Subsequent heating of **1a**−**1c** at higher temperature afforded the second isomer (**2a**−**2c**), showing formation of *cis-N,N′* orientation for the aforementioned cyclometalates. Further thermolysis of either *trans* or *cis*-Ir(III) complexes **1** or **2** in presence of sodium acetate, which serves as both activator and chloride scavenger, gave successful isolation of a mixture of two fully cyclometalated Ir(III) complexes *trans-N,N′*-[$(C^N)_2$Ir(dpn)] (**3a**−**3c**) and *cis-N,N′*-[$(C^N)_2$Ir(dpn)] (**4a**−**4c**). Structural and photophysical properties of complexes **3a**−**3c** and **4a**−**4c** were measured and compared. Time-dependent density functional theory (DFT) studies suggested that, upon changing the C^N cyclometalates from quinazolinyl, isoquinolinyl, and, finally, to pyridyl fragment, the lowest unoccupied molecular orbitals (LUMOs) are gradually shifted from the cyclometalating nitrogen heterocycles to the 1-naphthyl group of the phosphine chelate and, concomitantly altered the photophysical properties. An organic light-emitting diode (OLED) using orange-red phosphors **4a** and **4b** has been successfully fabricated. At the practical brightness of 500 $cd \cdot m^{-2}$, decent external quantum efficiency of 10.6% and 12.5% could be reached for **4a** and **4b**, respectively, revealing the usefulness of relevant molecular architecture in designing triplet OLED emitters.

Introduction

Organic light-emitting diodes (OLEDs) using either homoleptic or heteroleptic cyclometalated Ir(III) complexes that emit from their triplet metal-to-ligand charge-transfer (^{3}MLCT) states have received much current interest for applications in full color displays and solid state lighting because of the higher phosphorescent quantum efficiency.[1] These molecules allow efficient harvesting of electroluminescence originating from both singlet and triplet excitons; thus, 100% internal quantum efficiency can be achieved theoretically.[2] Therefore, highly efficient OLEDs have been reported by doping blue, green to red Ir(III) metal based phosphors in the small molecule host matrix or even the low molecular weight hole-conducting polymer.

In pursuing better Ir(III) phosphors for OLED application, one key requirement is to attain stable molecular assembly showing satisfactory emission quantum yields at room temperature. Many highly emissive Ir(III) metal complexes were then designed and synthesized, but the studies on relationships between structural and spectroscopic properties remain a major challenge.[3] The standard synthesis of

*To whom correspondence should be addressed. E-mail: ychi@mx.nthu.edu.tw (Y.C.), chop@ntu.edu.tw (P.-T.C.), wenhung@mail.ntou.edu.tw (W.-Y.H.).

(1) (a) Evans, R. C.; Douglas, P.; Winscom, C. J. *Coord. Chem. Rev.* **2006**, *250*, 2093. (b) Chou, P.-T.; Chi, Y. *Eur. J. Inorg. Chem.* **2006**, 3319. (c) Chi, Y.; Chou, P.-T. *Chem. Soc. Rev.* **2007**, *36*, 1421. (d) Williams, J. A. G.; Develay, S.; Rochester, D. L.; Murphy, L. *Coord. Chem. Rev.* **2008**, *252*, 2596. (e) Wong, W.-Y.; Ho, C.-L. *J. Mater. Chem.* **2009**, *19*, 4457. (f) You, Y.; Park, S. Y. *Dalton Trans.* **2009**, 1267. (g) Baranoff, E.; Yum, J.-H.; Grätzel, M.; Nazeeruddin, M. K. *J. Organomet. Chem.* **2009**, *694*, 2661. (h) Chi, Y.; Chou, P.-T. *Chem. Soc. Rev.* **2010**, *39*, 638.

(2) (a) Kwong, R. C.; Lamansky, S.; Thompson, M. E. *Adv. Mater.* **2000**, *12*, 1134. (b) Adachi, C.; Baldo, M. A.; Thompson, M. E.; Forrest, S. R. *J. Appl. Phys.* **2001**, *90*, 5048. (c) Sun, Y.; Giebink, N. C.; Kanno, H.; Ma, B.; Thompson, M. E.; Forrest, S. R. *Nature* **2006**, *440*, 908. (d) Thompson, M. E. *MRS Bull.* **2007**, *32*, 694. (e) Chou, P.-T.; Chi, Y. *Chem.—Eur. J.* **2007**, *13*, 380.

(3) (a) Wong, W.-Y.; Ho, C.-L. *Coord. Chem. Rev.* **2009**, *253*, 1709. (b) Murphy, L.; Williams, J. A. G. *Top. Organomet. Chem.* **2010**, *28*, 75. (c) Chen, Z.-Q.; Bian, Z.-Q.; Huang, C.-H. *Adv. Mater.* **2010**, *22*, 1534. (d) Ulbricht, C.; Beyer, B.; Friebe, C.; Winter, A.; Schubert, U. S. *Adv. Mater.* **2009**, *21*, 4418.

Published on Web 09/03/2010

emissive Ir(III) complexes is accomplished through a two-step process, in which the first step is known as the Nonoyama reaction that yields a chloride-bridged dimer $[(C^{\wedge}N)_2Ir(\mu\text{-}Cl)]_2$ with four cyclometalating C^N chelates.[4] After this, replacement of the chlorides with either the identical C^N chelate or using an ancillary chelating anion results in the formation of the desired, emissive complexes. If the third chelate is identical to the original C^N cyclometalates, the resulting complexes are named homoleptic, and otherwise, heteroleptic complexes. Typical heteroleptic complexes comprise stable ancillary chelates such as acetylacetonate (acac),[5] *N*-methyl salicylimine (sal),[5] picolinate (pic),[6] and functionalized azolate,[7] and in recently, the selection of ancillary chelates has been extended to the less accessible, tailor-made heterocycles such as dithiocarbamate,[8] dithiophosphate, and benzamidinate.[9]

Despite of the above-mentioned intensive examination, however, there are only a few reports that focus on the class of heteroleptic *tris*-cyclometalated Ir(III) complexes for which the third chelate is also derived from the carbanion based chelating ligands.[10] One particular important example is the red-emitting *mer*-$[Ir(piq)_2(ppy)]$ and $[Ir(ppy)_2(piq)]$, piqH = 1-phenylisoquinoline and ppyH = 2-phenylpyridine, which are synthesized using transmetalation between the respective Ir(III) dimers and organozinc reagents prepared in situ.[11] In searching for a better and more generalized methodology to synthesize these heteroleptic *tris*-cyclometalated complexes, we have been attracted by the facile cyclometalating power of benzyldiphenylphosphine ligand and its analogues,[12] and decided to synthesize the relevant Ir(III) phosphors by adopting these P^C cyclometalates.[13] Herein, we report the synthesis, structure and photophysics of new Ir(III) complexes $[(C^{\wedge}N)_2Ir(P^{\wedge}C)]$, for which the C^N chelates are 4-fluorophenylpyridine, 1-(4-fluorophenyl)isoquinoline, and 4-(4-fluorophenyl)quinazoline, while the P^C chelate is the cyclometalated diphenyl(1-naphthyl)phosphine. It is notable that the benzyl fragment of the original P^C chelate, that is, benzyldiphenylphosphine, is now replaced by the 1-naphthyl group in an attempt to circumvent its potentially higher chemical reactivity under the basic conditions, which could be detrimental to the device lifespan of as-fabricated OLEDs.[14]

Experimental Section

General Procedures. All reactions were performed under argon atmosphere and solvents were distilled from appropriate drying agents prior to use. Commercially available reagents were used without further purification unless otherwise stated. All reactions were monitored using precoated TLC plates (0.20 mm with fluorescent indicator UV254). Mass spectra were obtained on a JEOL SX-102A instrument operating in electron impact (EI) or fast atom bombardment (FAB) mode. ^1H and ^{13}C NMR spectra were recorded on a Varian Mercury-400 or an INOVA-500 instrument. Elemental analysis was carried out with a Heraeus CHN-O Rapid Elementary Analyzer. The N-heterocyclic aromatics, such as 4-(4-fluorophenyl)quinazoline (fnazoH), 1-(4-fluorophenyl)isoquinoline (fpiqH), and 4-fluorophenylpyridine (fppyH), were prepared from the reaction of 4-fluorobenzeneboronic acid with 4-chloroquinazoline, 1-chloroisoquinoline, and 1-bromopyridine under the conditions of Suzuki cross coupling. The synthetic procedures and spectroscopic data for fppyH and fpiqH cyclometalates are akin to those described in the literature.[15,16] The Ir(III) starting materials $[(fnazo)_2Ir(\mu\text{-}Cl)]_2$, $[(fppy)_2Ir(\mu\text{-}Cl)]_2$, and $[(fpiq)_2Ir(\mu\text{-}Cl)]_2$ were obtained from treatment of $IrCl_3 \cdot 3H_2O$ with approximately 2.5 equiv of fnazoH, fpiqH and fppyH, respectively;[17] while diphenyl(1-naphthyl)phosphine (dpnH) was prepared according to the literature methods.[18]

Photophysical and Electrochemical Measurements. Steady-state absorption and emission spectra were recorded with a Hitachi (U-3310) spectrophotometer and an Edinburgh (FS920) fluorimeter, respectively. Both the wavelength-dependent excitation and the emission response of the fluorimeter had been calibrated. Lifetime studies were performed with an Edinburgh FL 900 photon-counting system with a hydrogen-filled/or a nitrogen lamp as the excitation source. Data were analyzed using the nonlinear least-squares procedure in combination with an iterative convolution method. The emission decays were analyzed by the sum of exponential functions, which allows partial removal of the instrument time broadening and consequently renders a temporal resolution of ~200 ps. Solution samples were degassed by three freeze−pump−thaw cycles. The resulting luminescence was acquired by an intensified charge-coupled detector.

Cyclic voltammetry (CV) was performed using a CH instruments electrochemical analyzer. The oxidation and reduction potentials were recorded using glassy carbon and Au disk coated with Hg as working electrodes, respectively, in anhydrous CH_2Cl_2 and tetrahydrofuran (THF) with 0.1 M $TBAPF_6$ as

(4) Nonoyama, M. *Bull. Chem. Soc. Jpn.* **1974**, *47*, 767.
(5) Lamansky, S.; Djurovich, P.; Murphy, D.; Abdel-Razzaq, F.; Kwong, R.; Tsyba, I.; Bortz, M.; Mui, B.; Bau, R.; Thompson, M. E. *Inorg. Chem.* **2001**, *40*, 1704.
(6) Byun, Y.; Jeon, W. S.; Lee, T.-W.; Lyu, Y.-Y.; Chang, S.; Kwon, O.; Han, E.; Kim, H.; Kim, M.; Lee, H.-J.; Das, R. R. *Dalton Trans.* **2008**, 4732.
(7) (a) Coppo, P.; Plummer, E. A.; De Cola, L. *Chem. Commun.* **2004**, 1774. (b) Yeh, S.-J.; Wu, M.-F.; Chen, C.-T.; Song, Y.-H.; Chi, Y.; Ho, M.-H.; Hsu, S.-F.; Chen, C. H. *Adv. Mater.* **2005**, *17*, 285. (c) Hwang, F.-M.; Chen, H.-Y.; Chen, P.-S.; Liu, C.-S.; Chi, Y.; Shu, C.-F.; Wu, F.-I.; Chou, P.-T.; Peng, S.-M.; Lee, G.-H. *Inorg. Chem.* **2005**, *44*, 1344. (d) Lo, S.-C.; Harding, R. E.; Shipley, C. P.; Stevenson, S. G.; Burn, P. L.; Samuel, I. D. W. *J. Am. Chem. Soc.* **2009**, *131*, 16681. (e) Stagni, S.; Colella, S.; Palazzi, A.; Valenti, G.; Zacchini, S.; Paolucci, F.; Marcaccio, M.; Albuquerque, R. Q.; De Cola, L. *Inorg. Chem.* **2008**, *47*, 10509. (f) Chiu, Y.-C.; Chi, Y.; Hung, J.-Y; Cheng, Y.-M.; Yu, Y.-C.; Chung, M.-W.; Lee, G.-H.; Chou, P.-T.; Chen, C.-C.; Wu, C.-C.; Hsieh, H.-Y. *ACS Appl. Mater. Int.* **2009**, *1*, 433.
(8) Chen, L.; You, H.; Yang, C.; Zhang, X.; Qin, J.; Ma, D. *J. Mater. Chem.* **2006**, *16*, 3332.
(9) (a) Liu, Y.; Ye, K.; Fan, Y.; Song, W.; Wang, Y.; Hou, Z. *Chem. Commun.* **2009**, 3699. (b) Peng, T.; Bi, H.; Liu, Y.; Fan, Y.; Gao, H.; Wang, Y.; Hou, Z. *J. Mater. Chem.* **2009**, *19*, 8072.
(10) Dedeian, K.; Shi, J.; Shepherd, N.; Forsythe, E.; Morton, D. C. *Inorg. Chem.* **2005**, *44*, 4445.
(11) Huo, S.; Deaton, J. C.; Rajeswaran, M.; Lenhart, W. C. *Inorg. Chem.* **2006**, *45*, 3155.
(12) (a) Duff, J. M.; Shaw, B. L. *J. Chem. Soc., Dalton Trans.* **1972**, 2219. (b) Singleton, E.; van der Stok, E. *J. Chem. Soc., Dalton Trans.* **1978**, 926. (c) Bedford, R. B.; Hazelwood, S. L.; Horton, P. N.; Hursthouse, M. B. *Dalton Trans.* **2003**, 4164. (d) Beck, R.; Zheng, T.; Sun, H.; Li, X.; Floerke, U.; Klein, H.-F. *J. Organomet. Chem.* **2008**, *693*, 3471. (e) Djukic, J.-P.; Sortais, J.-B.; Barloy, L.; Pfeffer, M. *Eur. J. Inorg. Chem.* **2009**, 817.
(13) (a) Hung, J.-Y.; Chi, Y.; Pai, I.-H.; Cheng, Y.-M.; Yu, Y.-C.; Lee, G.-H.; Chou, P.-T.; Wong, K.-T.; Chen, C.-C.; Wu, C.-C. *Dalton Trans.* **2009**, 6472. (b) Chiu, Y.-C.; Lin, C.-H.; Hung, J.-Y.; Chi, Y.; Cheng, Y.-M.; Wang, K.-W.; Chung, M.-W.; Lee, G.-H.; Chou, P.-T. *Inorg. Chem.* **2009**, *48*, 8164. (c) Chiu, Y.-C.; Hung, J.-Y.; Chi, Y.; Chen, C.-C.; Chang, C.-H.; Wu, C.-C.; Cheng, Y.-M.; Yu, Y.-C.; Lee, G.-H.; Chou, P.-T. *Adv. Mater.* **2009**, *21*, 2221. (d) Hung, J.-Y.; Lin, C.-H.; Chi, Y.; Chung, M.-W.; Chen, Y.-J.; Lee, G.-H.; Chou, P.-T.; Chen, C.-C.; Wu, C.-C. *J. Mater. Chem.* **2010**, *20*, 7682.
(14) Vedernikov, A. N.; Huffman, J. C.; Caulton, K. G. *Inorg. Chem.* **2002**, *41*, 6244.
(15) Rho, H. H.; Park, Y. H.; Lee, Y. H.; Park, N. G.; Ha, Y.; Kim, Y. S. *Mol. Cryst. Liq. Cryst.* **2006**, *444*, 145.
(16) Liu, C.; Yang, W. *Chem. Commun.* **2009**, 6267.
(17) Song, Y.-H.; Yeh, S.-J.; Chen, C.-T.; Chi, Y.; Liu, C.-S.; Yu, J.-K.; Hu, Y.-H.; Chou, P.-T.; Peng, S.-M.; Lee, G.-H. *Adv. Funct. Mater.* **2004**, *14*, 1221.
(18) (a) Van Allen, D.; Venkataraman, D. *J. Org. Chem.* **2003**, *68*, 4590. (b) Gelman, D.; Jiang, L.; Buchwald, S. L. *Org. Lett.* **2003**, *5*, 2315.

the supporting electrolyte, at the scan rate of 50 $mV \cdot s^{-1}$. The potentials were measured against an Ag/Ag^+ (0.01 M $AgNO_3$) reference electrode with ferrocene as the external standard.

Synthesis of *trans-N,N′*-[(fnazo)$_2$Ir(dpnH)Cl] (1a). Diphenyl(1-naphthyl)phosphine (dpnH, 93 mg, 0.30 mmol) and [(fnazo)$_2$Ir(μ-Cl)]$_2$ (100 mg, 0.074 mmol) were added in decalin (15 mL), and the mixture was heated at 100 °C for 24 h. After cooling to room temperature (RT), the solvent was removed and residue was subjected to silica gel column chromatography using a 2:1 mixture of ethyl acetate and hexane as the eluent. Orange crystalline solids were obtained by slow diffusion of methanol into a CH_2Cl_2 solution at RT (120 mg, 0.12 mmol, 82%). The orange *trans-N,N′*-[(fpiq)$_2$Ir(dpnH)Cl] (**1b**) and yellow *trans-N,N′*-[(fppy)$_2$Ir(dpnH)Cl] (**1c**) were prepared from the reaction of dpnH with [(fnazo)$_2$Ir(μ-Cl)]$_2$ and with [(fnazo)$_2$Ir(μ-Cl)]$_2$ under similar conditions. Yields: 80% for **1b** and 82% for **1c**.

Spectral Data of 1a. MS (FAB, ^{192}Ir): m/z 987 $(M+1)^+$, 951 $(M-Cl)^+$. ^{1}H NMR (500 MHz, CD_2Cl_2, 298 K): δ 9.52 (s, 1H), 9.22 (s, 1H), 8.82 (d, J = 8.5 Hz, 1H), 8.41−8.36 (m, 2H), 8.28 (dd, J = 9.3, 5.8 Hz, 1H), 8.07 (d, J = 8.0 Hz, 1H), 7.97 (td, J = 7.8, 1.5 Hz, 1H), 7.83 (td, J = 7.8, 1.5 Hz, 1H), 7.77 (t, J = 7.3 Hz, 1H), 7.69 (d, J = 8.0 Hz, 1H), 7.63 (t, J = 6.8 Hz, 2H), 7.43 (d, J = 7.0 Hz, 2H), 7.37 (t, J = 6.8 Hz, 2H), 7.30 (t, J = 7.3 Hz, 2H), 7.22−7.21 (m, 4H), 7.11−7.00 (m, 4H), 6.83 (td, J = 8.8, 2.5 Hz, 1H), 6.75 (td, J = 8.8, 2.5 Hz, 3H), 5.90 (dd, J = 9.5, 3.0 Hz, 1H), 5.72−5.69 (m, 1H). ^{19}F NMR (470 MHz, CD_2Cl_2, 298 K): δ −106.31 (s, 1F), −106.90 (s, 1F). ^{31}P NMR (202 MHz, CD_2Cl_2, 298 K): δ −4.46 (br). Anal. Calcd. for $C_{50}H_{33}ClF_2IrN_4P$: C, 60.88; H, 3.37; N, 5.68. Found: C, 60.46; H, 3.55; N, 5.60.

Selected crystal data of **1a**: $C_{50}H_{33}ClF_2IrN_4P$; M = 986.42; monoclinic; space group = $P2_1/n$; a = 11.8495(9) Å, b = 14.1968(9) Å, c = 23.0295(15) Å, β = 93.446(2)°; V = 3867.1(5) Å^3; Z = 4; ρ_{calcd} = 1.694 mg m^{-3}; $F(000)$ = 1952; crystal size = 0.26 × 0.20 × 0.08 mm^3; λ(Mo−K$_\alpha$) = 0.71073 Å; T = 150(2) K; μ = 3.617 mm^{-1}; 20943 reflections collected, 8852 independent reflections (R_{int} = 0.0471), GOF = 1.022, final $R_1[I > 2\sigma(I)]$ = 0.0375 and wR_2(all data) = 0.0785.

Spectral Data of 1b. MS (FAB, ^{192}Ir): m/z 949 $(M-Cl)^+$. ^{1}H NMR (500 MHz, CD_2Cl_2, 298 K): δ 8.89−8.87 (m, 2H), 8.60 (d, J = 6.5 Hz, 1H), 8.50 (d, J = 8.0 Hz, 1H), 8.21 (t, J = 7.0 Hz, 1H), 8.15 (dd, J = 6.0, 3.0 Hz, 1H), 7.89 (d, J = 8.5 Hz, 2H), 7.79−7.74 (m, 3H), 7.60−7.53 (m, 3H), 7.44 (d, J = 7.5 Hz, 3H), 7.33 (t, J = 7.0 Hz, 1H), 7.24 (t, J = 7.0 Hz, 2H), 7.18−7.17 (m, 3H), 7.12 (d, J = 7.0 Hz, 1H), 7.05 (br, 2H), 6.96 (br, 2H), 6.84 (br, 2H), 6.73 (td, J = 8.5, 2.0 Hz, 1H), 6.65 (td, J = 8.5, 2.5 Hz, 1H), 6.50−6.47 (m, 1H), 5.75 (d, J = 9.5 Hz, 1H), 5.64 (dd, J = 10.0, 2.5 Hz, 1H). ^{19}F NMR (470 MHz, CD_2Cl_2, 298 K): δ −110.91 (s, 1F), −111.23 (s, 1F). ^{31}P NMR (202 MHz, CD_2Cl_2, 298 K): δ −2.84 (br). Anal. Calcd. for $C_{52}H_{35}ClF_2IrN_2P$: C, 63.44; H, 3.58; N, 2.85. Found: C, 62.99; H, 3.80; N, 2.81.

Spectral Data of 1c. MS (FAB, ^{192}Ir): m/z 884 $(M)^+$, 849 $(M-Cl)^+$. ^{1}H NMR (500 MHz, CD_2Cl_2, 298 K): δ 8.87 (d, J = 5.5 Hz, 1H), 8.82 (d, J = 6.0 Hz, 1H), 7.86 (d, J = 8.0 Hz, 2H), 7.78−7.73 (m, 2H), 7.65−7.62 (m, 1H), 7.53−7.50 (m, 3H), 7.35 (br, 2H), 7.30 (t, J = 7.0 Hz, 4H), 7.16−7.13 (m, 4H), 7.04 (t, J = 6.5 Hz, 2H), 6.95 (br, 3H), 6.82 (td, J = 6.0, 1.0 Hz, 1H), 6.63 (td, J = 8.8, 2.5 Hz, 1H), 6.59 (td, J = 8.8, 2.5 Hz, 1H), 6.27 (br, 1H), 5.38−5.35 (m, 2H). ^{19}F NMR (470 MHz, CD_2Cl_2, 298 K): δ −109.98 (s, 1F), −110.95 (s, 1F). ^{31}P NMR (202 MHz, CD_2Cl_2, 298 K): δ −3.85 (br). Anal. Calcd. for $C_{44}H_{31}ClF_2IrN_2P$: C, 59.76; H, 3.53; N, 3.17. Found: C, 59.84; H, 3.88; N, 3.35.

Synthesis of *cis-N,N′*-[(fnazo)$_2$Ir(dpnH)Cl] (2a). Diphenyl(1-naphthyl)phosphine (dpnH, 93 mg, 0.30 mmol) and [(fnazo)$_2$Ir(μ-Cl)]$_2$ (100 mg, 0.074 mmol) were added in decalin (15 mL), and the mixture was heated at a much higher temperature of 170 °C for 40 h. After cooling to RT, the solvent was removed, and residue was subjected to silica gel column chromatography using a 2:1 mixture of ethyl acetate and hexane as the eluent. Orange-red crystalline solids were obtained by slow diffusion of methanol into a CH_2Cl_2 solution at RT (**2a**, 93 mg, 0.94 mmol, 64%).

Spectral Data of 2a. MS (FAB, ^{192}Ir): m/z 987 $(M+1)^+$, 951 $(M-Cl)^+$. ^{1}H NMR (400 MHz, CD_2Cl_2, 298 K): δ 9.36 (br, 1H), 8.82 (d, J = 8.4 Hz, 1H), 8.43 (dd, J = 8.8, 6.0 Hz, 2H), 8.18 (br, 1H), 7.89−7.73 (m, 5H), 7.65 (br, 2H), 7.41−6.77 (m, 20H), 5.96 (br, 1H). ^{19}F NMR (376 MHz, CD_2Cl_2, 298 K): δ −106.88 (s, 1F), −107.62 (s, 1F). ^{31}P NMR (202 MHz, CD_2Cl_2, 298 K): δ −5.08 (br). Anal. Calcd. for $C_{50}H_{33}ClF_2IrN_4P$: C, 60.88; H, 3.37; N, 5.68. Found: C, 60.39; H, 3.58; N, 5.64.

Selected Crystal Data of 2a. $C_{51}H_{35}Cl_3F_2IrN_4P$; M = 1071.35; triclinic; space group = $P\bar{1}$; a = 12.8852(6) Å, b = 20.4021(10) Å, c = 25.3648(12) Å, α = 102.351(1)°, β = 101.616(1)°, γ = 96.608(1)°; V = 6292.5(5) Å^3; Z = 6; ρ_{calcd} = 1.696 mg m^{-3}; $F(000)$ = 3180; crystal size = 0.25 × 0.20 × 0.20 mm^3; λ(Mo−K$_\alpha$) = 0.71073 Å; T = 150(2) K; μ = 3.464 mm^{-1}; 82616 reflections collected, 28866 independent reflections (R_{int} = 0.0524), GOF = 0.993, final $R_1[I > 2\sigma(I)]$ = 0.0436 and wR_2(all data) = 0.1140.

Conversion of 1a to 2a. A solution of **1a** (100 mg, 0.101 mmol) in decalin (15 mL) was heated at 170 °C for 30 h. After cooling to RT, the solvent was removed under vacuum, and residue was subjected to silica gel column chromatography to afford two major components, which are identified as **1a** (4 mg, 0.004 mmol, 4%) and **2a** (71 mg, 0.72 mmol, 71%). The control reactions for **1b** and **1c** produce similar result, and the data is thus skipped to avoid redundancy.

Synthesis of *trans-* and *cis-N,N′*-[(fnazo)$_2$Ir(dpn)] (3a) and (4a). To a 25 mL of reaction flask, diphenyl(1-naphthyl)phosphine (dpnH, 93 mg, 0.297 mmol), [(fnazo)$_2$Ir(μ-Cl)]$_2$ (100 mg, 0.074 mmol), and sodium acetate (61 mg, 0.742 mmol) were added in decalin (10 mL), and the mixture was brought to reflux for 18 h. Following cooling to RT, solvent was removed under vacuum, and the residue was subjected to silica gel column chromatography using a 1:2 mixture of ethyl acetate and hexane as the eluent, giving 23 mg of *trans-N,N′*-[(fnazo)$_2$Ir(dpn)] (**3a**, 0.024 mmol, 16%) and 65 mg of *cis-N,N′*-[(fnazo)$_2$Ir(dpn)] (**4a**, 0.068 mmol, 46%). Orange single crystals of both complexes were obtained by slow diffusion of methanol into a CH_2Cl_2 solution at RT. The alternative reaction using identical ratio of reactants, but conducted in refluxing xylenes for 125 h, afforded **3a** and **4a** in 33 and 34% of yields, respectively.

Spectral Data of 3a. MS (FAB, ^{192}Ir): m/z 951 $(M+1)^+$. ^{1}H NMR (500 MHz, DMSO, 298 K): δ 8.92 (d, J = 8.5 Hz, 1H), 8.63 (t, J = 6.5 Hz, 1H), 8.51 (d, J = 9.0 Hz, 1H), 8.41 (dd, J = 9.0, 5.0 Hz, 1H), 8.36 (d, J = 1.5 Hz, 2H), 8.07 (t, J = 7.0 Hz, 2H), 7.97−7.84 (m, 6H), 7.79−7.74 (m, 2H), 7.70 (td, J = 7.5, 2.0 Hz, 1H), 7.56−7.49 (m, 4H), 7.03 (t, J = 7.5 Hz, 1H), 6.96 (td, J = 8.8, 2.5 Hz, 1H), 6.88 (td, J = 8.8, 2.5 Hz, 1H), 6.73 (d, J = 6.0 Hz, 1H), 6.58 (dd, J = 8.8, 2.5 Hz, 1H), 6.47 (td, J = 7.5, 2.0 Hz, 2H), 6.39 (t, J = 7.5 Hz, 1H), 6.14−6.07 (m, 3H). ^{19}F NMR (376 MHz, DMSO, 298 K): δ −106.84 (d, J_{FP} = 5.64 Hz, 1F), −107.94 (s, 1F). ^{31}P NMR (202 MHz, DMSO, 298 K): δ 21.14 (d, J_{FP} = 5.46 Hz). Anal. Calcd. for $C_{50}H_{32}F_2IrN_4P$: C, 63.21; H, 3.40; N, 5.90. Found: C, 62.78; H, 3.72; N, 5.68.

Spectral Data of 4a. MS (FAB, ^{192}Ir): m/z 951 $(M+1)^+$. ^{1}H NMR (500 MHz, $CDCl_3$, 298 K): δ 8.77 (d, J = 9.0 Hz, 1H), 8.51 (s, 1H), 8.30−8.22 (m, 3H), 8.12 (dd, J = 10.8, 7.0 Hz, 2H), 8.03 (dd, J = 9.0, 5.0 Hz, 1H), 7.95−7.87 (m, 3H), 7.81 (td, J = 7.5, 1.0 Hz, 1H), 7.75−7.69 (m, 3H), 7.56−7.51 (m, 2H), 7.47−7.44 (m, 2H), 7.39 (td, J = 7.8, 2.0 Hz, 2H), 7.07−7.01 (m, 2H), 6.70 (d, J = 7.0 Hz, 1H), 6.62 (td, J = 8.5, 2.5 Hz, 2H), 6.49 (dt, J = 11.5, 2.0 Hz, 1H), 6.35−6.32 (m, 2H), 6.27−6.23 (m, 3H). ^{19}F NMR (470 MHz, $CDCl_3$, 298 K): δ −108.87 (s, 1F), −109.07 (s, 1F). ^{31}P NMR (202 MHz, $CDCl_3$, 298 K): δ 24.53 (s). Anal. Calcd. for $C_{50}H_{32}F_2IrN_4P$: C, 63.21; H, 3.40; N, 5.90. Found: C, 62.88; H, 3.73; N, 5.80.

Selected Crystal Data of 4a. $C_{51}H_{34}Cl_2F_2IrN_4P$; M = 1034.89; monoclinic; space group = $P2_1/c$; a = 22.0192(10) Å,

b = 9.4220(4) Å, c = 21.6136(10) Å, β = 115.095(1)°; V = 4060.8(3) Å^3; Z = 4; ρ_{calcd} = 1.693 mg m^{-3}; $F(000)$ = 2048; crystal size = 0.23 × 0.20 × 0.08 mm^3; λ(Mo−K$_\alpha$) = 0.71073 Å; T = 150(2) K; μ = 3.512 mm^{-1}; 26054 reflections collected, 9315 independent reflections (R_{int} = 0.0455), GOF = 1.049, final R$_1$[$I > 2\sigma(I)$] = 0.0376 and wR$_2$(all data) = 0.0835.

Synthesis of *trans*- and *cis*-*N*,*N*′-[(fpiq)$_2$Ir(dpn)] (3b) and (4b). To a 25 mL of reaction flask, diphenyl(1-naphthyl)phosphine (dpnH, 93 mg, 0.297 mmol), [(fpiq)$_2$Ir(μ-Cl)]$_2$ (100 mg, 0.074 mmol), and sodium acetate (61 mg, 0.742 mmol) were added in decalin (10 mL), and the mixture was brought to reflux for 18 h. Following cooling to RT, solvent was removed under vacuum, and the residue was subjected to silica gel column chromatography using a 1:2 mixture of ethyl acetate and hexane as the eluent, giving 19 mg of *trans*-*N*,*N*′-[(fpiq)$_2$Ir(dpn)] (**3b**, 0.020 mmol, 13%) and 62 mg of *cis*-*N*,*N*′-[(fpiq)$_2$Ir(dpn)] (**4b**, 0.065 mmol, 44%). The alternative reaction using identical ratio of reagents, but conducted in refluxing xylenes for 125 h, afforded **3b** and **4b** in 41 and 21% of yields, respectively.

Spectral Data of 3b. MS (FAB, ^{192}Ir): m/z 948 (M)$^+$. ^{1}H NMR (500 MHz, CD_2Cl_2, 298 K): δ 8.84 (d, J = 8.5 Hz, 1H), 8.45 (m, 1H), 8.29 (t, J = 6.0 Hz, 1H), 8.10 (dd, J = 9.0, 5.5 Hz, 1H), 7.96−7.91 (m, 4H), 7.82 (d, J = 7.0 Hz, 1H), 7.76 (d, J = 6.5 Hz, 1H), 7.67−7.63 (m, 3H), 7.59−7.57 (m, 2H), 7.55−7.52 (m, 2H), 7.46 (d, J = 8.0 Hz, 1H), 7.42 (d, J = 6.5 Hz, 1H), 7.35 (t, J = 6.5 Hz, 2H), 7.03 (t, J = 7.5 Hz, 1H), 6.84 (d, J = 6.5 Hz, 1H), 6.76 (td, J = 8.8, 3.0 Hz, 1H), 6.71 (d, J = 6.5 Hz, 1H), 6.67 (dd, J = 8.8, 3.0 Hz, 1H), 6.53 (d, J = 7.0 Hz, 1H), 6.47 (dd, J = 8.8, 2.5 Hz, 1H), 6.34−6.33 (m, 3H), 6.27−6.23 (m, 3H). ^{19}F NMR (376 MHz, CD_2Cl_2, 298 K): δ −112.71 (d, J_{FP} = 5.64 Hz, 1F), −113.44 (s, 1F). ^{31}P NMR (202 MHz, CD_2Cl_2, 298 K): δ 22.79 (d, J_{FP} = 5.46 Hz). Anal. Calcd. for $C_{52}H_{34}F_2IrN_2P$: C, 65.88; H, 3.61; N, 2.95. Found: C, 65.38; H, 4.09; N, 3.02.

Spectral Data of 4b. MS (FAB, ^{192}Ir): m/z 948 (M)$^+$. ^{1}H NMR (500 MHz, $CDCl_3$, 298 K): δ 8.84 (d, J = 9.5 Hz, 1H), 8.40 (d, J = 8.0 Hz, 1H), 8.15−8.12 (m, 2H), 8.08 (dd, J = 8.5, 6.0 Hz, 1H), 7.91 (d, J = 7.5 Hz, 1H), 7.89−7.84 (m, 3H), 7.68−7.60 (m, 4H), 7.53−7.47 (m, 5H), 7.44−7.40 (m, 2H), 7.35 (td, J = 8.0, 2.0 Hz, 2H), 7.10 (dd, J = 9.0, 2.5 Hz, 1H), 7.02−7.00 (m, 1H), 6.96 (d, J = 6.5 Hz, 1H), 6.75−6.74 (m, 2H), 6.55−6.46 (m, 2H), 6.23−6.18 (m, 5H). ^{19}F NMR (470 MHz, $CDCl_3$, 298 K): δ −112.58 (s, 1F), −112.80 (s, 1F). ^{31}P NMR (202 MHz, $CDCl_3$, 298 K): δ 24.59 (s). Anal. Calcd. for $C_{52}H_{34}F_2IrN_2P$: C, 65.88; H, 3.61; N, 2.95. Found: C, 65.66; H, 3.86; N, 3.17.

Synthesis of *trans*- and *cis*-*N*,*N*′-[(fppy)$_2$Ir(dpn)] (3c) and (4c). To a 25 mL of reaction flask, diphenyl(1-naphthyl)phosphine (dpnH, 110 mg, 0.350 mmol), [(fppy)$_2$Ir(μ-Cl)]$_2$ (100 mg, 0.087 mmol), and sodium acetate (72 mg, 0.874 mmol) were added in decalin (10 mL), and the mixture was brought to reflux for 18 h. Following cooling to RT, solvent was removed under vacuum, and the residue was subjected to silica gel column chromatography using a 1:3 mixture of ethyl acetate and hexane as the eluent, giving 81 mg of yellow *trans*-*N*,*N*′-[(fppy)$_2$Ir(dpn)] (**3c**, 0.096 mmol, 55%) and 43 mg of *cis*-*N*,*N*′-[(fppy)$_2$Ir(dpn)] (**4c**, 0.051 mmol, 29%). The alternative reaction using identical ratio of reagents, but conducted in refluxing xylenes for 63 h, afforded **3c** and **4c** in 78 and 5% of yields, respectively.

Spectral Data of 3c. MS (FAB, ^{192}Ir): m/z 849 (M+1)$^+$. ^{1}H NMR (400 MHz, CD_2Cl_2, 298 K): δ 8.07 (d, J = 6.0 Hz, 1H), 7.95−7.89 (m, 4H), 7.77−7.70 (m, 3H), 7.58−7.54 (m, 2H), 7.49−7.40 (m, 6H), 7.38 (t, J = 9.2 Hz, 1H), 7.03 (t, J = 7.4 Hz, 1H), 6.93 (t, J = 7.8 Hz, 2H), 6.72−6.63 (m, 4H), 6.51 (dd, J = 8.8, 2.4 Hz, 1H), 6.34−6.25 (m, 4H), 5.83−5.69 (m, 1H). ^{19}F NMR (376 MHz, $CDCl_3$, 298 K): δ −111.61 (d, J_{FP} = 6.77 Hz, 1F), −113.04 (s, 1F). ^{31}P NMR (202 MHz, $CDCl_3$, 298 K): δ 21.11 (d, J_{FP} = 6.46 Hz). Anal. Calcd. for $C_{44}H_{30}F_2IrN_2P$: C, 62.33; H, 3.57; N, 3.30. Found: C, 62.22; H, 3.83; N, 3.67.

Selected Crystal Data of 3c. $C_{46}H_{34}Cl_4F_2IrN_2P$; M = 1017.72; monoclinic; space group = $P2_1$; a = 9.6454(6) Å, b = 13.9259(8) Å, c = 14.9197(8) Å, β = 90.161(1)°; V = 2004.0(2) Å^3; Z = 2; ρ_{calcd} = 1.687 mg m^{-3}; $F(000)$ = 1004; crystal size = 0.26 × 0.18 × 0.02 mm^3; λ(Mo−K$_\alpha$) = 0.71073 Å; T = 150(2) K; μ = 3.684 mm^{-1}; 19919 reflections collected, 8540 independent reflections (R_{int} = 0.0508), GOF = 1.046, final R$_1$[$I > 2\sigma(I)$] = 0.0391 and wR$_2$(all data) = 0.0975.

Spectral Data of 4c. MS (FAB, ^{192}Ir): m/z 849 (M+1)$^+$. ^{1}H NMR (400 MHz, d^6-acetone, 298 K): δ 8.20 (t, J = 8.8 Hz, 2H), 8.04 (d, J = 8.0 Hz, 1H), 7.97−7.92 (m, 2H), 7.78−7.73 (m, 5H), 7.58−7.53 (m, 2H), 7.48 (d, J = 5.6 Hz, 1H), 7.43−7.39 (m, 4H), 6.99−6.92 (m, 3H), 6.88 (dd, J = 9.2, 2.8 Hz, 1H), 6.74−6.71 (m, 2H), 6.65−6.63 (m, 2H), 6.60−6.55 (m, 2H), 6.48 (td, J = 8.6, 2.4 Hz, 1H), 6.17 (t, J = 9.2 Hz, 2H). ^{19}F NMR (470 MHz, $CDCl_3$, 298 K): δ −113.00 (s, 1F), −113.32 (s, 1F). ^{31}P NMR (202 MHz, $CDCl_3$, 298 K): δ 22.00 (s). Anal. Calcd. for $C_{44}H_{30}F_2IrN_2P$: C, 62.33; H, 3.57; N, 3.30. Found: C, 62.04; H, 3.83; N, 3.28.

Selected Crystal Data of 4c. $C_{45}H_{32}Cl_2F_2IrN_2P$; M = 932.80; triclinic; space group = $P\bar{1}$; a = 9.4505(6) Å, b = 12.3390(8) Å, c = 17.2315(11) Å, α = 87.351(1)°, β = 77.387(1)°, γ = 71.201(1)°; V = 1855.6(2) Å^3; Z = 2; ρ_{calcd} = 1.669 mg m^{-3}; $F(000)$ = 920; crystal size = 0.25 × 0.22 × 0.22 mm^3; λ(Mo−K$_\alpha$) = 0.71073 Å; T = 150(2) K; μ = 3.831 mm^{-1}; 24029 reflections collected, 8493 independent reflections (R_{int} = 0.0299), GOF = 1.059, final R$_1$[$I > 2\sigma(I)$] = 0.0255 and wR$_2$(all data) = 0.0624.

Cyclometalation of 1a. A mixture of **1a** (100 mg, 0.101 mmol) and sodium acetate (42 mg, 0.507 mmol) in xylenes (10 mL) was refluxed for 120 h. After cooling to RT, the solvent was removed under vacuum, and residue was subjected to silica gel column chromatography as before to afford a mixture of 22 mg of **3a** (0.023 mmol, 23%) and 43 mg of **4a** (0.045 mmol, 45%).

Cyclometalation of 2a. A mixture of **2a** (100 mg, 0.101 mmol) and sodium acetate (42 mg, 0.507 mmol) in xylenes (10 mL) was refluxed for 120 h. After cooling to RT, the solvent was removed under vacuum, and residue was subjected to silica gel column chromatography as before to afford a mixture of 22 mg of **3a** (0.023 mmol, 23%) and 52 mg of **4a** (0.055 mmol, 54%).

X-ray Diffraction Studies. Single crystal X-ray diffraction data of **1a**, **2a**, **3c**, **4a**, and **4c** were measured on a Bruker SMART Apex CCD diffractometer using (Mo−K$_\alpha$) radiation (λ = 0.71073 Å). The data collection was executed using the SMART program. Cell refinement and data reduction were performed with the SAINT program. The structure was determined using the SHELXTL/PC program and refined using full-matrix least-squares.[19]

Computational Methodology. Geometry optimizations of all studied complexes were carried out using the density functional theory (DFT) with the B3LYP hybrid functional.[20] A "double-ζ" quality basis set consisting of Hay and Wadt's effective core potentials (LANL2DZ)[21] was employed for Ir atom, and a 6-31G* basis set,[22] for H, C, N, F, and P atoms. The relativistic effective core potential (ECP) replaced the inner core electrons of Ir(III) metal atom, leaving the outer core (5s^{2}5p^6) electrons and the 5d^6 valence electrons to be concerned with. Time-dependent DFT (TD-DFT)[23]

(19) (a) Sheldrick, G.-M. *SHELXL97, Program for the refinement of crystal structure*; University of Göttingen: Göttingen, Germany, 1997. (b) *SHELXTL*, V6.1; BrukerAXS, Inc: Madison, WI, 2000.

(20) (a) Lee, C.; Yang, W.; Parr, R. G. *Phys. Rev. B* **1988**, *37*, 785. (b) Becke, A. D. *J. Chem. Phys.* **1993**, *98*, 5648.

(21) (a) Hay, P. J.; Wadt, W. R. *J. Chem. Phys.* **1985**, *82*, 270. (b) Wadt, W. R.; Hay, P. J. *J. Chem. Phys.* **1985**, *82*, 284. (c) Hay, P. J.; Wadt, W. R. *J. Chem. Phys.* **1985**, *82*, 299.

(22) Hariharan, P. C.; Pople, J. A. *Mol. Phys.* **1974**, *27*, 209.

(23) (a) Jamorski, C.; Casida, M. E.; Salahub, D. R. *J. Chem. Phys.* **1996**, *104*, 5134. (b) Petersilka, M.; Grossmann, U. J.; Gross, E. K. U. *Phys. Rev. Lett.* **1996**, *76*, 1212. (c) Bauernschmitt, R.; Ahlrichs, R.; Hennrich, F. H.; Kappes, M. M. *J. Am. Chem. Soc.* **1998**, *120*, 5052. (d) Casida, M. E. *J. Chem. Phys.* **1998**, *108*, 4439. (e) Stratmann, R. E.; Scuseria, G. E.; Frisch, M. J. *J. Chem. Phys.* **1998**, *109*, 8218.

calculations using the B3LYP functional were then performed based on the optimized structures at ground states in combination with an integral equation formalism-polarizable continuum model, IEF-PCM (in dichloromethane).[24] Typically, the lowest 10 triplet and singlet roots of the non-hermitian eigenvalue equations were obtained to determine the vertical excitation energies. Oscillator strengths were deduced from the dipole transition matrix elements (for singlet states only). All calculations were carried out using Gaussian 03.[25]

The compositions of molecular orbitals in terms of the constituent chemical fragments were calculated using the AOMix program.[26] For the characterization of the HOMO-x → LUMO+y transitions as partial charge transfer (CT) transitions, the following definition of the CT character has been used:

$$\mathrm{CT(M)} = \%\mathrm{(M)HOMO\text{-}x} - \%\mathrm{(M)LUMO{+}y}$$

where %(M)HOMO-x and %(M)LUMO+y are electronic densities on the metal in the HOMO-x and the LUMO+y. If the excited state, for example, S_1 or T_1, is formed by more than one one-electron excitation, then the metal CT character of this excited state is expressed as a sum of CT characters of each participating excitation, $i \rightarrow j$:

$$\mathrm{CT_I(M)} = \sum_{i,\,a} [\mathrm{C_I}(i \rightarrow j)]^2 (\%(\mathrm{M})_i - \%(\mathrm{M})_j)$$

where $C_I(i \rightarrow j)$ are the appropriate coefficients of the I-th eigenvector of the configuration interaction (CI) matrix.

Device Fabrication and Measurement. OLEDs were fabricated by vacuum deposition of the materials at 10^{-6} Torr onto ITO-coated glass substrates having a sheet resistance of 15 Ω square^{-1}. The ITO surface was cleaned through ultrasonication sequentially with acetone, methanol, and deionized water, followed by the treatment with UV-ozone. Poly(3,4-ethylenedioxythiophene)-poly(4-stylenesurfonate) (PEDOT:PSS) was spin-coated onto the substrates to serve as the hole-injection layer and dried at 130 °C for 30 min to remove residual water. Organic layers were then vacuum deposited at a deposition rate of about 1−2 Å·s^{-1}. Subsequently, LiF was deposited at 0.1 Å·s^{-1} and then capped with Al (ca. 5 Å s^{-1}) by shadow masking without breaking the vacuum. The current−voltage−brightness (I−V−L) characteristics of the devices were measured simultaneously using a Keithley 6430 source meter and a Keithley 6487 picoammeter equipped with a calibration Si-photodiode. Electroluminescence (EL) spectra were measured using an Ocean Optics spectrometer.

Results and Discussion

Synthesis and Characterization. Three heterocyclic ligands with distinctive π-conjugation and energy gaps between the highest occupied molecular orbital (HOMO) and the lowest unoccupied molecular orbital (LUMO), fnazo, fpiq, and fppy, were conveniently synthesized by using the Suzuki cross coupling reaction employing fluorine substituted 4-fluorobenzeneboronic acid and the respective aryl halide. Cyclometalated Ir(III) chloride bridged dimers, namely, $[(\mathrm{fnazo})_2\mathrm{Ir}(\mu\text{-Cl})]_2$, $[(\mathrm{fpiq})_2\mathrm{Ir}(\mu\text{-Cl})]_2$, and $[(\mathrm{fppy})_2\mathrm{Ir}(\mu\text{-Cl})]_2$, were then synthesized by $IrCl_3 \cdot n H_2O$ with approximately 2.5 equiv of these aromatic heterocycles. After then, the chloride-bridged dimer complexes

Scheme 1

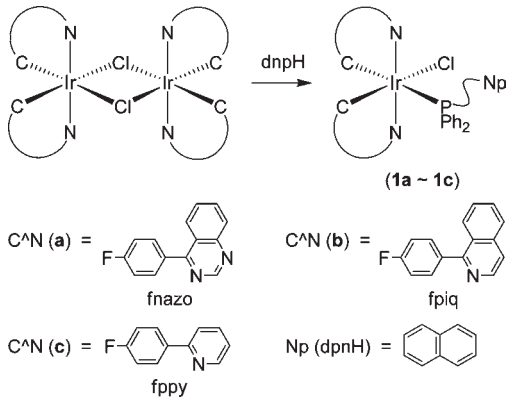

can be easily converted to mononuclear Ir(III) complexes by addition of diphenyl(1-naphthyl)phosphine at 100 °C for 24 h, giving formation of the first series of Ir(III) complexes (**1a**−**1c**), with retention of the original chelate conformation during transformation (Scheme 1). Elemental analysis of **1a**−**1c** is consistent with the proposed formulation (see Experimental Section). The mass spectrum of all derivatives gives the anticipated molecular ion peaks, while spectroscopic studies show well-resolved multiplets for the C^N cyclometalates in the ^{1}H NMR spectra, together with the complementary ^{31}P NMR signal of coordinated diphenyl(1-naphthyl)phosphine.

Subsequent heating of complexes **1a**−**1c** in decalin afforded the second isomer (**2a**−**2c**), showing the isomerization around the metal core skeleton and formation of the *cis*-N,N' orientation for the chelating cyclometalates. Apparently, phosphine coordination activates the Ir(III) metal center, for which the observed skeletal isomerization is somewhat related to the recently reported isomerization of N,N'-*trans*-iridium(III)[bis(4,6-difluorophenylpyridinato) (2-carboxy-4-dimethylamino pyridine)] to its N,N'-*cis* counterpart during sublimation.[27] Using the fnazo substituted **a** derivatives as representative example, further thermolysis of either *trans* or *cis*-Ir(III) metal complexes **1** or **2** in presence of sodium acetate, which serves as both activator and chloride scavenger by forming insoluble NaCl precipitate, gave isolation of a mixture of two distinctive, fully cyclometalated Ir(III) metal complexes **3** and **4** (Scheme 2). It is notable that these complexes exhibited the respective N,N'-*trans* and *cis*- orientation imposed by the dual C^N chelates in a way similar to that of their precursors **1** and **2**.

Moreover, the N,N'-*cis* isomer **2a** seems to be the thermodynamic product for the simple phosphine addition reaction. This is demonstrated by the exclusive formation of **2a** over **1a** upon increasing the reaction temperature to 170 °C. It is notable that, in all isomers **1**, there are two stronger field ligands, that is, carbon and phosphorus donor groups, which are located at the energetically unfavorable, mutual *trans*-disposition. The retention of C^N chelate conformation in **1** then confirmed its nature as the kinetic product of the phosphine addition reaction. Subsequently, isomerization to isomers **2** then placed both carbon and phosphorus

(24) Cancès, M. T.; Mennucci, B.; Tomasi, J. *J. Chem. Phys.* **1997**, *107*, 3032.
(25) *Gaussian 03*, revision C.02; Gaussian, Inc.: Wallingford, CT, 2004.
(26) (a) Gorelsky, S. I. *AOMix: Program for Molecular Orbital Analysis*; University of Ottawa: Ottawa, Ontario, Canada, 2007; http://www.sg chem.net/. (b) Gorelsky, S. I.; Lever, A. B. P. *J. Organomet. Chem.* **2001**, *635*, 187.
(27) Baranoff, E.; Suarez, S.; Bugnon, P.; Barolo, C.; Buscaino, R.; Scopelliti, R.; Zuppiroli, L.; Graetzel, M.; Nazeeruddin, M. K. *Inorg. Chem.* **2008**, *47*, 6575.

Scheme 2[a]

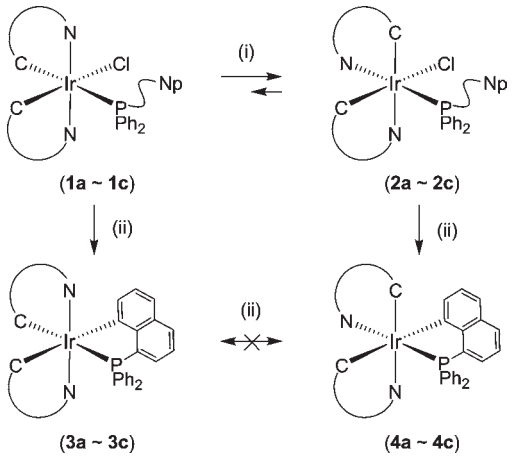

[a] **Reaction conditions: (i) 170 °C, 48 h; (ii) NaOAc, 190 °C, 18 h.**

donors at the position opposite to the weak field ligands such as nitrogen aromatics and chloride, providing the thermodynamic driving force.

On the other hand, similar to the treatment of $[(fnazo)_2Ir(\mu\text{-}Cl)]_2$ with dpnH phosphine in presence of sodium acetate, heating a pure sample of either **1a** or **2a** with sodium acetate afforded a mixture of **3a** and **4a**, for which the control experiments showed no interconversion between **3a** and **4a** under similar conditions. This observation is best interpreted by a prior substitution of acetate for chloride, which not only induced isomerization, forming complexes with ligand conformation analogous to that of **1a** and **2a**, but also promoted subsequent cyclometalation, affording a mixture of products **3a** and **4a**. Such isomerization processes are highly sensitive to the reaction temperatures and the starting materials, that is, either complexes **1**, **2**, or respective Ir(III) dimers employed. The combination of these factors explains the large difference in product yields for reactions conducted under variable temperatures. Table 1 shows the yields of isomeric complexes **3** and **4** isolated from the reactions of Ir(III) dimer and diphenyl(1-naphthyl)phosphine at two distinctive temperatures. It is notable that lower boiling-point xylene solution always favors the formation of **3**, for which their *N*,*N*′-*trans*-ligand arrangement is identical to that of the parent Ir(III) dimer and/or complexes **1**. In other words, the reactions are under kinetic control.

Finally, we also made several attempts to extend the synthetic scope by applying non-fluorinated heterocycles such as 2-phenyl pyridine, 1-phenyl isoquinoline, and 4-phenyl quinazoline as initial C^N cyclometalates, or using benzyldiphenylphosphine as the third P^C ancillary chelate. To our surprise, none of these reactions gave the anticipated Ir(III) products in reasonable quantities, showing a delicate balance among reactivity, stability, and electronic properties of all cyclometalating chelates. This observation also demonstrates a rare case that the 4-fluorophenyl fragment seems to affect the stability of the cyclometalated Ir(III) complexes.[28]

Table 1. Synthesis of Ir(III) Phosphors from the Respective Chloride-Bridged Ir(III) Dimer and Diphenyl(1-naphthyl)phosphine in Presence of Sodium Acetate

starting materials	temp. (°C)	time (h)	yields
$[(fnazo)_2Ir(\mu\text{-}Cl)]_2$	~190	18	**3a**: 16%; **4a**: 46%
$[(fnazo)_2Ir(\mu\text{-}Cl)]_2$	~142	125	**3a**: 33%; **4a**: 34%
$[(fpiq)_2Ir(\mu\text{-}Cl)]_2$	~190	18	**3b**: 13%; **4b**: 44%
$[(fpiq)_2Ir(\mu\text{-}Cl)]_2$	~142	125	**3b**: 41%; **4b**: 21%
$[(fppy)_2Ir(\mu\text{-}Cl)]_2$	~190	18	**3c**: 55%; **4c**: 29%
$[(fppy)_2Ir(\mu\text{-}Cl)]_2$	~142	63	**3c**: 78%; **4c**: 5%

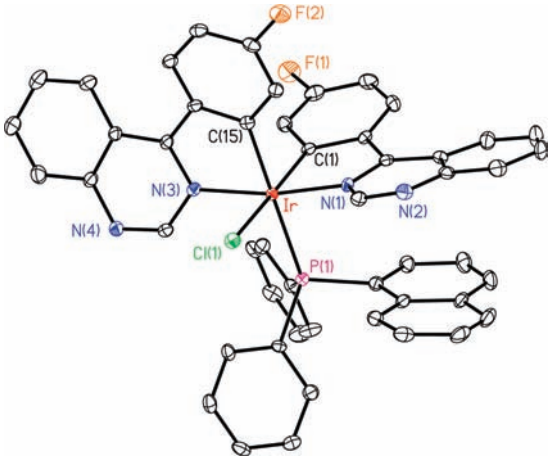

Figure 1. ORTEP diagram of **1a** with thermal ellipsoids shown at 30% probability level. Selected bond distances: Ir−C(1) = 2.007(4), Ir−C(15) = 2.026(4), Ir−N(1) = 2.040(3), Ir−N(3) = 2.068(3), Ir−P(1) = 2.451(1), Ir−Cl(1) = 2.474(1) Å.

Crystal Structures. The crystal structures of complexes **1a**, **2a**, **3c**, **4a**, and **4c** were determined by X-ray crystallography to reveal the coordination arrangement of these Ir(III) metal complexes. As depicted in Figures 1 and 2, the pyridyl fragment of the fnazo ligands in **1a** and **2a** are in mutual *trans* and *cis* disposition. One remarkable variation of metric parameters lies in the shortening of the unique P−Ir distance from 2.451 Å in **1a** to 2.304 Å in **2a**, which can be rationalized by the pronounced *trans*-effect of phenyl group of fnazo ligands, while the Ir−Cl distances remain essentially unaltered (2.474 and 2.465 Å), since both the chloride ligands retained the position *trans* to the cyclometalated phenyl group. Moreover, in both complexes, the naphthyl group of the phosphine showed parallel arrangement to one fnazo chelate, for which the centroid-centroid contact between the inner hexagonal ring of naphthyl and quinazolinyl fragment is calculated to be 3.494 and 3.366 Å, respectively. Such non-negligible intraligand $\pi\pi$ stacking interaction was also observed in similar cyclometalate Ir(III) complexes bearing 2-(diphenylphosphino)phenolate chelate,[29] except that, in the current examples, our structural results showed a higher preference for the naphthyl versus the phenyl groups of phosphine in forming the intramolecular $\pi\pi$ stacking interaction with respect to the cyclometalate chelates.

The X-ray structural analysis on **3c** was next examined. It is notable that the fppy chelates adopts the *N*,*N*′-*trans*-arrangement, which is similar to that of fnazo chelates in **1a**, along with the replacement of chloride with the

(28) (a) Grushin, V. V.; Herron, N.; LeCloux, D. D.; Marshall, W. J.; Petrov, V. A.; Wang, Y. *Chem. Commun.* **2001**, 1494. (b) Babudri, F.; Farinola, G. M.; Naso, F.; Ragni, R. *Chem. Commun.* **2007**, 1003.

(29) Lee, T.-C.; Chang, C.-F.; Chiu, Y.-C.; Chi, Y.; Chan, T.-Y.; Cheng, Y.-M.; Lai, C.-H.; Chou, P.-T.; Lee, G.-H.; Chien, C.-H.; Shu, C.-F.; Leonhardt, J. *Chem. Asian J.* **2009**, *4*, 742.

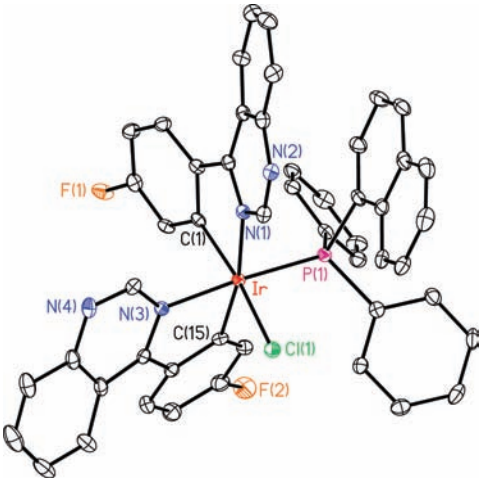

Figure 2. ORTEP diagram of **2a** with thermal ellipsoids shown at 30% probability level. Selected bond distances: Ir−C(1) = 2.001(5), Ir−C(15) = 2.020(5), Ir−N(1) = 2.148(4), Ir−N(3) = 2.092(4), Ir−P(1) = 2.304(1), Ir−Cl(1) = 2.465(1) Å.

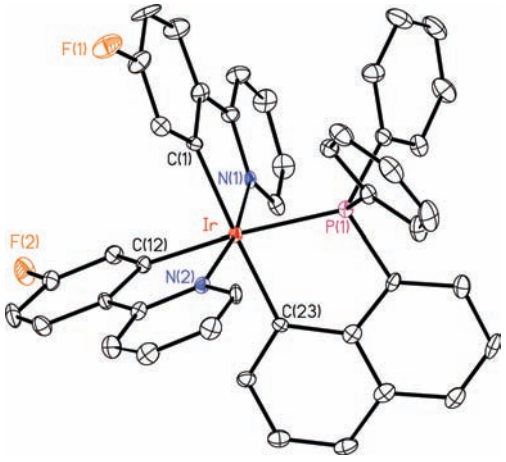

Figure 3. ORTEP diagram of **3c** with thermal ellipsoids shown at 30% probability level. Selected bond distances: Ir−C(1) = 2.065(7), Ir−C(12) = 2.034(7), Ir−C(23) = 2.115(6), Ir−N(1) = 2.056(5), Ir−N(2) = 2.057(6), Ir−P(1) = 2.330(2) Å.

cyclometalated naphthyl fragment for completing the octahedral geometry (Figure 3). Moreover, the Ir−C distance that resides *trans* to the cyclometalated naphthyl fragment now increases to 2.065(7) Å in **3c** from 2.007(4) Å in **1a**, which is residing *trans* to the chloride, but the respective Ir−C distance *trans* to the phosphine remains unchanged (2.026(4) Å in **1a** and 2.034(7) Å in **3c**). Concomitantly, the Ir−C(23) bond of the naphthyl group in **3c** is measured to be 2.115(6) Å because of the strong competition exerted by the *trans*-ppy group.

Finally, the X-ray structural determination of **4a** and **4c** was conducted for revealing the ligand arrangement of *N*,*N*′-*cis*-isomers. As shown in Figures 4 and 5, except that the quinazoline fragments in **4a** are slightly distorted as in **1a** and **2a**, both complexes still have all cyclometalated carbon donors adopting the meridional configuration, which is identical to that of *trans*-complexes **3a**−**3c**. It is also notable that the Ir−N distances in **4a** are marginally shorter than those in **4c**, indicating that the basicity of imine could play a pivotal role in stabilizing the

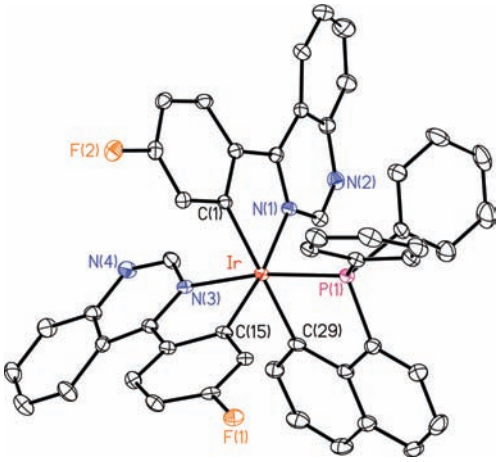

Figure 4. ORTEP diagram of **4a** with thermal ellipsoids shown at 30% probability level. Selected bond distances: Ir−C(1) = 2.086(4), Ir−C(15) = 2.013(4), Ir−C(29) = 2.121(4), Ir−N(1) = 2.126(3), Ir−N(3) = 2.082(3), Ir−P(1) = 2.247(1) Å.

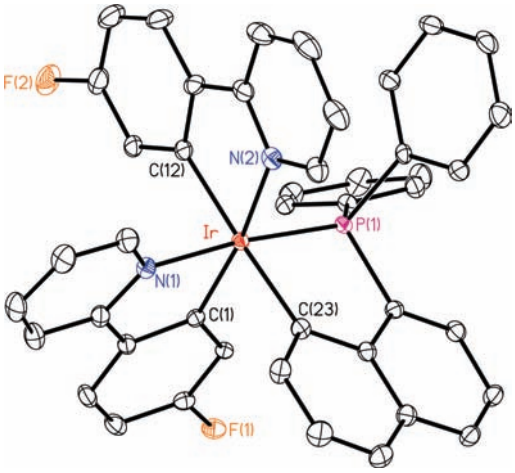

Figure 5. ORTEP diagram of **4c** with thermal ellipsoids shown at 30% probability level. Selected bond distances: Ir−C(1) = 2.018(3), Ir−C(12) = 2.081(3), Ir−C(23) = 2.109(3), Ir−N(1) = 2.103(2), Ir−N(2) = 2.143(3), Ir−P(1) = 2.243(1) Å.

final emissive complexes.[5,30] Moreover, the nitrogen atoms of C^N cyclometalates occupy the mutual *cis*-dispositions, while the PPh_2 donor of dpn chelate is in the *cis* position to one nitrogen atom, which is consistent with the thermodynamic driving force for reducing the *trans*-effect. In the case of **4c**, a remarkable character is the significant lengthening of the Ir−N distances (cf. Ir−N(1) = 2.103(2) and Ir−N(2) = 2.143(3) Å), which are located *trans* to the phosphorus and carbon atoms, respectively. However, the Ir−N distances of the respective *N*,*N*′-*trans*-isomer **3c** are much shorter because of the weakened *trans*-effect exerted by the nitrogen atoms (cf. Ir−N(1) = 2.056(5) and Ir−N(2) = 2.057(6) Å). Notably, the Ir−C and Ir−P distances for the dpn chelate in **3c** (Ir−C(23) = 2.115(6) and Ir−P(1) = 2.330(2) Å) show minor variation to Ir−C(23) = 2.109(3) and Ir−P(1) = 2.243(1) Å in **4c**. This change in the Ir−P distance may be ascribed to the influence of their *trans* atoms, that is, carbon atom in **3c** and nitrogen atom in **4c**.

(30) Ren, X.; Giesen, D. J.; Rajeswaran, M.; Madaras, M. *Organometallics* **2009**, *28*, 6079.

Table 2. Selected Photophysical Properties of Ir (III) Complexes **3a**−**4c** Recorded in CH_2Cl_2 Solution and Respective Electrochemical Data

	abs. λ_{max}/nm ($\varepsilon \times 10^{-3}$)	em. λ_{max} (nm)	Q.Y.	τ_{obs} (μs)	k_r (s^{-1})	k_{nr} (s^{-1})	redn. $E_{1/2}$ (ΔE_p)[a]	oxdn. E_{pa} (ΔE_p)[b]
3a	288 (33.0), 348 (22.8), 441 (10.0)	638	0.016	0.046	3.45×10^5	2.12×10^7	−1.98 (75), −2.19 (83)	0.56 (irr)
3b	280 (41.0), 351 (20.5), 429 (8.3)	650	0.41	4.59	8.90×10^4	1.28×10^5	−2.36 (70), −2.56 (62)	0.38 (irr)
3c	357 (18.5)	534, 573	0.21	71.7	2.93×10^3	1.10×10^4	−2.83 (76)	0.42 (irr)
4a	292 (29.7), 349 (21.9), 476 (5.2)	628	0.11	0.36	3.05×10^5	2.47×10^6	−2.00 (88), −2.20 (83)	0.56 (irr)
4b	292 (34.3), 355 (19.2), 441 (6.1)	582, 619	~1	8.46	1.18×10^5	0	−2.40 (85), −2.58 (74)	0.42 (95)
4c	354 (9.9)	540, 574	0.24	74.9	3.20×10^3	1.01×10^4	−2.86 (66)	0.42 (78)

[a] (i) The oxidation and reduction experiments were conducted in CH_2Cl_2 and THF solution, respectively. (ii) Redn. $E_{1/2}$ refers to $[(E_{pa} + E_{pc})/2]$, in which E_{pa} and E_{pc} are the anodic and cathodic peak potentials referenced to the Fc^+/Fc couple in V, while $\Delta E_p = |E_{pa} - E_{pc}|$ was reported in mV. [b] Anodic oxdn. peak potential E_{pa} was quoted for both the reversible and irreversible process, ΔE_p = irr.

Electrochemical Properties. Electrochemical analysis via cyclic voltammetry (CV) was performed to obtain the redox potentials of all complexes **3** and **4**, for which the electrochemical data are summarized in Table 2. For complexes **3a**, **3b**, **4a**, and **4b**, each displays two reversible reduction waves between −1.98/−2.40 V and −2.19/−2.58 V ranges, respectively. The observed peak patterns are similar to what were found for typical heteroleptic Ir(III) complexes, confirming that the reductions occur on the cyclometalated C^N ligands. This assignment is in good agreement with the results of DFT calculations (vide infra). In sharp contrast, the ppy complexes **3c** and **4c** show only one broadened reduction peak at higher potential of −2.83 V and −2.86 V, respectively. This process is then assigned to the reduction of either fppy cyclometalates or even naphthyl moiety of chelating phosphine because both groups are expected to have a higher lying π^*-orbital energy. Moreover, for the measurement of oxidation potentials, complexes **3a**, **3b**, **3c**, and **4a** showed an anodic peak potential spanning the narrow range of 0.38−0.56 V, while complexes **4b** and **4c** exhibit a reversible oxidation couple with $E_{1/2}$ = 0.37 and 0.38 V (or E_{pa} = 0.42 and 0.42 V), respectively, which can be assigned to the metal-based oxidation.

Moreover, our data also reveal that both the reduction and oxidation of the fnazo-based Ir(III) compounds **3a** and **4a** occur at significantly less negative potentials than are found for typical fpiq-based Ir(III) complexes **3b** and **4b**. The unique redox properties observed between these Ir(III) complexes are believed to result from the strong electron withdrawing abilities of the quinazoline versus that of isoquinoline, suggesting that fnazo complexes **3a** and **4a** may mainly act as electron-trapping instead of hole-trapping fragments when used as phosphorescent dopants in conventional OLED architectures.

Photophysical Properties. The absorption and emission spectra of these three sets of geometrical isomers (**3a**/**4a**, **3b**/**4b**, and **3c**/**4c**) recorded in degassed CH_2Cl_2 at room temperature are shown in Figure 6, and the pertinent data are summarized in Table 2. As shown in Figure 6, the intense absorption bands of all complexes in the higher-energy region (< 300 nm), with extinction coefficient (ε) being on the order of ~10^4 $M^{-1} \cdot cm^{-1}$, most probably originate from the ligand centered $\pi\pi^*$ transitions. The broad band at longer wavelength of up to 500 nm, as supported by their relatively lower extinction coefficients, is assigned to the tail of $\pi\pi^*$ transition overlapping with the metal-to-ligand charge transfer transition (MLCT) in the singlet manifold.

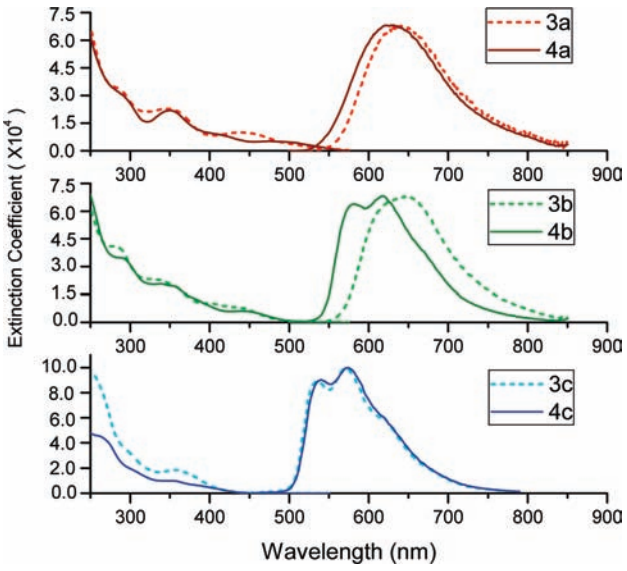

Figure 6. Absorption and luminescence spectra of **3a**−**4c** recorded in degassed CH_2Cl_2 at room temperature.

As for the emission spectra, the significant variation of emission intensity between aerated and degassed solution ensures the emission originating from the triplet manifold, that is, the phosphorescence. Depending on the C^N cyclometalates, their ligand orientation and overall geometry, distinct emission properties among these complexes are observed and summarized as follows: (i) Complexes **3a** and **4a** exhibit a smooth and broad emission with peak maximized at ~630 nm, while others show notable vibronic progression. (ii) Except for **3c** and **4c** with approximately equal emission gap, the emission of **4a** and **4b** series are significantly blue-shifted with respect to their isomers **3a** and **3b** (see Figure 6). (iii) The calculated radiative lifetimes for **3c** (341 μs, $k_r = 2.93 \times 10^3$ s^{-1}) and **4c** (312 μs, $k_r = 3.20 \times 10^3$ s^{-1}, see Table 2) are exceedingly long compared with those of all other studied complexes. (iv) The photophysical data listed in Table 2 clearly reveal a trend that quantum yield (Q.Y.) for **4a**, **4b**, and **4c** are all larger than those of their isomers **3a**, **3b**, and **3c**, respectively. Conversely, the nonradiative decay rate constant, k_{nr}, values are relatively small for **4a**, **4b**, and **4c** (cf. **3a**, **3b**, and **3c**, respectively). As a representative example, the phosphorescence of **4b** was exceedingly efficient, as indicated by its near unitary Q.Y. in fully degassed CH_2Cl_2 solution at room temperature. Conversely, the Q.Y. of **3a** is the lowest, only 0.016, among all titled complexes.

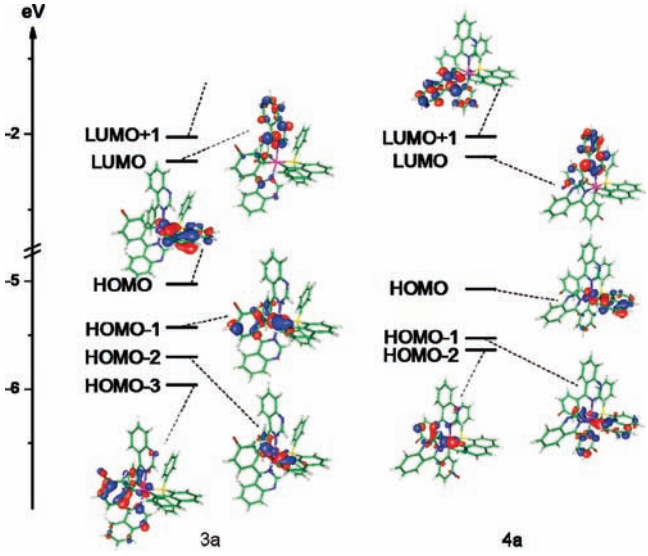

Figure 7. Selected frontier orbitals involved in the lower-lying electronic transitions for **3a** and **4a**.

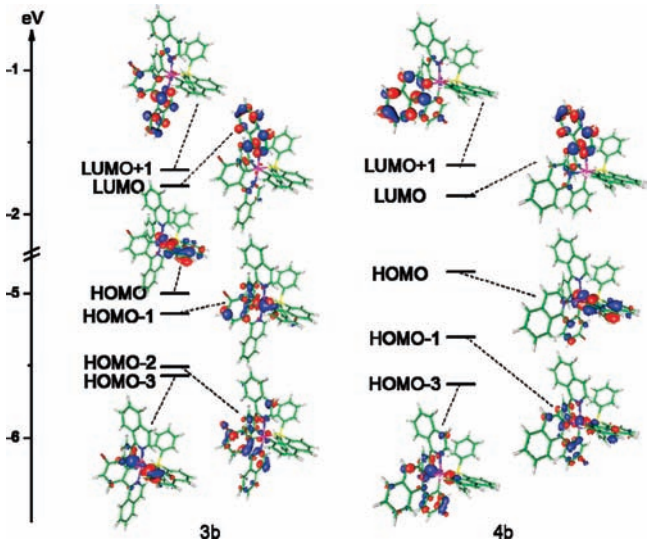

Figure 8. Selected frontier orbitals involved in the lower-lying electronic transitions for **3b** and **4b**.

DFT Calculations. The above-mentioned spectral features and corresponding relaxation dynamics imply their remarkable differences in the lower-lying electronic transition. Accordingly, time-dependent DFT incorporated with the PCM model to take the solvation effect into consideration has been performed to gain more insight into the fundamental basis of the electronic transitions (see Experimental Section for details). Figures 7−9 depict the selected molecular orbitals involved in the lower-lying transitions of these complexes. Table 3 lists all pertinent energy gaps calculated and corresponding assignments of each transition. Taking **3a** and **4a** as an example, the order of the calculated energy gaps of the $S_0 \rightarrow T_1$ absorption (554 and 550 nm for **3a** and **4a**, respectively) is in the same trend as the $T_1 \rightarrow S_0$ emission peak wavelength (**3a**: 638 nm, **4a**: 628 nm) recorded in CH_2Cl_2 solution (see Table 2). Similar results are obtained for the rest of complexes.

As for the transition characteristics, frontier orbital analyses indicate that for **3a** and **4a**, in view of phosphorescence, the $S_0 \rightarrow T_1$ transitions are primarily attributed to HOMO → LUMO (**3a**) and HOMO → LUMO+1 (**4a**) (see Table 3 and Figure 7), in which HOMOs of **3a** and **4a** are mainly localized at the central metal atom, and naphthyl moiety of the ancillary phosphine chelate, while the electron density of LUMO and LUMO+1 is distributed at the quinazolinyl moiety of the fnazo chelates. Therefore, the $S_0 \rightarrow T_1$ transition for **3a** and **4a** involves concomitantly MLCT and the ligand-to-ligand charge transfer (LLCT) characteristics. In comparison to that of **3a** and **4a**, the difference in transition character is resolved for **3b** and **4b**, in which the $S_0 \rightarrow T_1$ transition are MLCT (from metal d_π to isoquinolinyl moiety of the fpiq chelate) mixed mainly with intraligand charge transfer (ILCT) within the fpiq chelate, that is, from fluoro-phenyl to isoquinolinyl moiety. This distinction can be attributed to the weaker electron-withdrawing ability of isoquinolinyl moiety of **3b** and **4b** versus that of quinazolinyl moiety of **3a** and **4a**. The net result is to lift the energy level of fluorophenyl orbital and reduce the participation of the naphthyl part of the cyclometalated phosphine in the $S_0 \rightarrow T_1$ transition for **3b** and **4b**. As for the third series

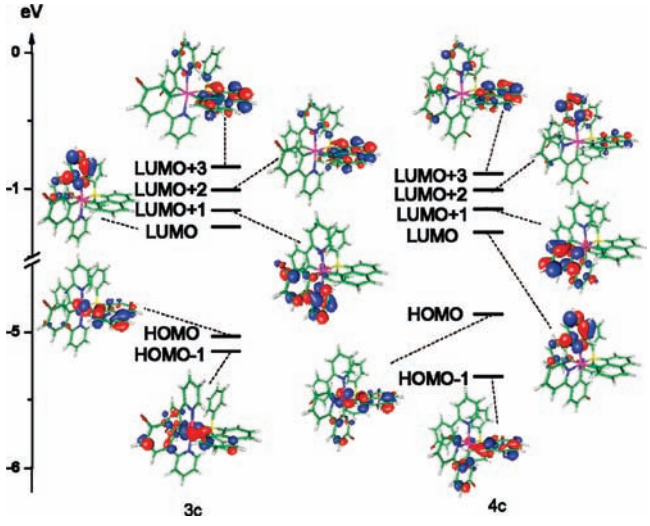

Figure 9. Selected frontier orbitals involved in the lower-lying electronic transitions for **3c** and **4c**.

of complexes **3c** and **4c**, the $\pi\pi^*$ energy gap for fppy is even larger than the naphthyl group of ancillary phosphine, which is the reverse of that observed in quinazolinyl and isoquinolinyl counterparts, and hence the emissions mainly originate from MLCT and ILCT within the naphthyl moiety; compare HOMO → LUMO+2 and HOMO → LUMO+3 for **3c** and **4c**, respectively (See Table 3 and Figure 9). These results correlate well with the observed emission spectral feature, in which **3a** and **4a** exhibit a smooth and broad emission because of the LLCT transition character, while the more localized ILCT transition in **3c** and **4c** exhibit notable vibronic progression.

The theoretical approaches also rationalize well the distinct blue shift of the emission for the **4a** and **4b** as compared to their geometry isomer of **3a** and **3b**. According to the calculation, the Ir−P distance for **3a** (2.434 Å) and **3b** (2.447 Å) is significantly longer than that for **4a** (2.316 Å) and **4b** (2.329 Å), respectively (see Table 4). The results, in theory, can be rationalized by the structural *trans* effect from $Ir-C_{(phenyl)}$ site exerting on the

Table 3. Calculated Energy Levels, Oscillator Strengths (*f*) and Orbital Transition Analyses of Ir(III) Complexes **3a**−**4c**

complexes	states	λ_{cal}	assignments	MLCT (%)
3a	T_1	554.04	HOMO → LUMO (47%) HOMO-3 → LUMO+1 (15%) HOMO → LUMO+1 (15%) HOMO-1 → LUMO (13%) HOMO-2 → LUMO (6%)	18.12%
	S_1	522.15	HOMO → LUMO (95%)	19.02%
4a	T_1	550.34	HOMO → LUMO+1 (58%) HOMO → LUMO (23%) HOMO-1 → LUMO+1 (9%) HOMO-2 → LUMO+1 (6%)	24.18%
	S_1	518.92	HOMO → LUMO (96%)	25.44%
3b	T_1	556.7	HOMO-2 → LUMO+1 (39%) HOMO → LUMO+1 (25%) HOMO → LUMO (12%) HOMO-1 → LUMO (8%) HOMO-1 → LUMO+1 (7%) HOMO-3 → LUMO+1 (6%)	14.84%
	S_1	464.81	HOMO → LUMO (89%) HOMO-1 → LUMO (6%)	22.84%
4b	T_1	553.57	HOMO→ LUMO+1 (30%) HOMO → LUMO (26%) HOMO-1 → LUMO+1 (21%) HOMO-1 → LUMO (11%) HOMO-3 → LUMO+1 (15%)	23.17%
	S_1	489.02	HOMO → LUMO (97%)	29.33%
3c	T_1	490.74	HOMO → LUMO+2 (53%) HOMO → LUMO+3 (17%) HOMO-1 → LUMO+2 (14%)	23.53%
	S_1	391.55	HOMO → LUMO (84%) HOMO-1 → LUMO (12%)	24.99%
4c	T_1	492.72	HOMO → LUMO+3 (42%) HOMO-1 → LUMO+3 (24%) HOMO → LUMO+2 (20%) HOMO-1 → LUMO+2 (10%)	21.68%
	S_1	407.37	HOMO → LUMO (97%)	31.35%

Table 4. Selected Geometrical Parameters for Ir(III) Complexes **3a**−**4c** Obtained from the Theoretical Calculations

	3a	**3b**	**3c**	**4a**	**4b**	**4c**
Ir−P (Å)	2.434	2.447	2.427	2.316	2.329	2.317

phosphine fragment. Accordingly, because of the reduced back-electron transfer to the phosphine in **3a** and **3b**, the central Ir(III) metal atoms are expected to be more electron rich, lifting their d_π orbital energy. Such a structural distinction results in the red shift emission for **3a** and **3b** compared with that of **4a** and **4b**. As for **3c** and **4c**, because the ILCT for the lowest lying transition is located at ancillary naphthyl moiety, the structural *trans* effect should have negligible influence on the phosphorescence, consistent with the nearly identical emission gap between **3c** and **4c** (see Figure 6). This viewpoint is reaffirmed by the CV measurements (see Table 2), in which the oxidation potential of 0.38 V for **3b** is slightly smaller than that of 0.42 V for **4b**.

In addition, the geometrical difference for each of the three sets of isomers (**3a**/**4a**, **3b**/**4b**, and **3c**/**4c**) also leads to an interesting influence on their emission yield and hence relaxation dynamics because of the structural *trans* effect. In each set of isomers, the strongest Ir−P bonding occurred with its *trans*-ligand being switched from the $Ir-C_{(phenyl)}$ site of geometrical isomers **3** to the quinazoline/isoquinoline/pyridine fragment of the respective isomers **4** (Table 4). Knowing that the strongly coordinated phosphines are able to further destabilize the metal-centered dd excited states, thereby decreasing the nonradiative processes. Accordingly, the k_{nr} values (quantum yields) for **4a**, **4b**, and **4c** are all smaller (larger) than those of their isomers **3a**, **3b**, and **3c**, respectively (see Table 2).

Finally, it is notable that the π-orbitals of the naphthyl chromophore, with an additional space provided by the phosphine, reside relatively far away from the Ir(III) metal atom. Theoretically, spin−orbit coupling is inversely proportional to distance (r) to the six power (according to a qualitative approach for a hydrogen like atom),[31] in which r is the distance between Ir and the ancillary chromophore. Therefore, despite the good percentage of MLCT (>20%), **3c** and **4c** are expected to have weaker heavy atom-induced spin−orbit coupling, giving a less allowed T_1-S_0 transition and hence a smaller radiative rate constant k_r. This viewpoint is evidenced by the k_r value for **3c** and **4c** of $\sim 10^3\ s^{-1}$, which is smaller than that of **3a**/**4a** and **3b**/**4b** by more than one order of the magnitude. Moreover, the dominant ILCT property for such lowest lying $S_0 \rightarrow T_1$ transitions, especially for **3c**/**4c** in which the π-electron is fully delocalized around the naphthyl moiety, also rationalizes the appearance of the vibronic emission profile observed in both **3c** and **4c**.

OLED Fabrication. In consideration of their higher photoluminescence (PL) efficiencies, shorter emission lifetimes, and higher synthetic yields, **4a** and **4b** were selected as dopants in the fabrication of multilayer OLEDs with configuration: ITO/PEDOT:PSS (30 nm)/NPB (15 nm)/TCTA (5 nm)/NSN and 8 wt % **4a** or **4b** (25 nm)/TPBI (50 nm)/LiF (0.5 nm)/Al (100 nm). This device architecture resembles those reported in the literature,[32] for which PEDOT:PSS and 4,4′-bis[*N*-(1-naphthyl)-*N*-phenylamino]-biphenyl (NPB) were functioned as the hole injection layer and the hole transport layer, respectively; while 4,5-diaza-2′,7′-bis(1-naphthylphenylamino)-9,9′-spirobifluorene (NSN) with suitable triplet energy (E_T = 2.38 eV) was selected as the host material.[33] For further improving the efficiency and reduction of the hole-injection barrier between NPB and the emitting layer, a thin layer of 4,4′,4″-tris-(*N*-carbazolyl)triphenylamine (TCTA) was inserted because of its intermediate HOMO energy level,[34] and 1,3,5-tris-(*N*-phenylbenzimidizol-2-yl)benzene (TPBI) was functioned as both hole-blocking and electron-transporting layer, whereas lithium fluoride (LiF) was used as the electron-injection material. Finally, the device was completed by depositing a thin layer of aluminum which served as the cathode. The overall device performances are then summarized in Table 5.

As shown in Figure 10a, the current density−voltage−luminance ($I-V-L$) characteristics of both devices are nearly the same, indicating that complexes **4a** and **4b** have very little influence on the charge transport characteristics. The $I-V$ and $L-V$ curves both show a steep upward increase reaching the turn-on voltage of 2 V, and the

(31) McGlynn, S. P.; Azumi, T.; Kinoshita, M. *Molecular Spectroscopy of the Triplet State*; Prentice Hall, Inc.: Englewood Cliffs, NJ, 1969.
(32) (a) Mi, B. X.; Wang, P. F.; Gao, Z. Q.; Lee, C. S.; Lee, S. T.; Hong, H. L.; Chen, X. M.; Wong, M. S.; Xia, P. F.; Cheah, K. W.; Chen, C. H.; Huang, W. *Adv. Mater.* **2009**, *21*, 339. (b) Tsai, T.-C.; Hung, W.-Y.; Chi, L.-C.; Wong, K.-T.; Hsieh, C.-C.; Chou, P.-T. *Org. Electron.* **2009**, *10*, 158. (c) Chi, L.-C.; Hung, W.-Y.; Chiu, H.-C.; Wong, K.-T. *Chem. Commun.* **2009**, 3892.
(33) Hung, W.-Y.; Wong, K.-T.; unpublished results.
(34) Su, S.-J.; Gonmori, E.; Sasabe, H.; Kido, J. *Adv. Mater.* **2008**, *20*, 4189.

Table 5. EL Performance of OLED Devices

dopant	V_{on} [V][a]	L = 500 nit [V, %]	L_{max} [cd·m^{-2}]	I_{max} [mA·cm^{-2}]	max. η_{EQE} [%]	max. η_l [cd·A^{-1}]	max. η_p [lm·W^{-1}]
4a	2	4.2, 10.6	51,700 (13.5 V)	1900	11.3	20.5	25.5
4b	2	3.7, 12.5	22,100 (11.3 V)	1250	14.4	30.6	33.3

[a] At a brightness of 0.01 cd m^{-2}.

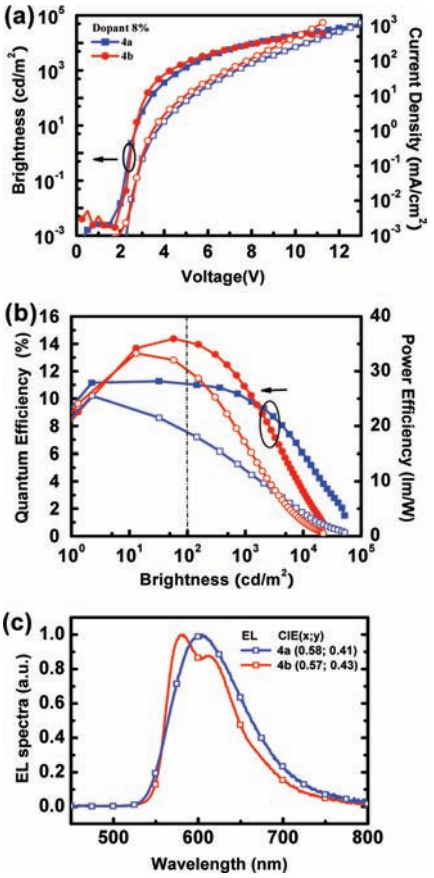

Figure 10. (a) Current density−voltage−luminance (I−V−L) characteristics. (b) External quantum (η_{EQE}) and power efficiencies as a function of brightness. (c) Normalized EL spectra of the devices.

degree of increase gradually slowed down at 500 cd·m^{-2}, for which the driving voltage is approximately 4.2 and 3.7 V for **4a** and **4b**, respectively. Figure 10b presents the external quantum efficiency and power efficiency as a function of luminance. The maximum values of η_{EQE} = 14.4%, η_l = 30.6 cd·A^{-1}, and η_p = 33.3 lm·W^{-1} for **4b** are significantly better than those of the **4a**-based device (η_{EQE} = 11.3%, η_l = 20.5 cd·A^{-1}, and η_p = 25.5 lm·W^{-1}). It is notable that, at the practical brightness of 500 cd·m^{-2}, the external quantum efficiency of **4b** remained as high as 12.5%, which is higher than that of 10.6% observed for **4a**. On the other hand, despite of the lower peak efficiency, the efficiency roll-off of **4a** is less serious than that of **4b**, although it is somewhat anticipated for all phosphorescent OLEDs at higher brightness. Figure 10c depicts the EL spectra of both phosphors at the bias of 5 V, which are identical to the solution PL spectra and displaying Commission Internationale de I'Eclairage (CIE) coordinates of (0.58, 0.41) and (0.57, 0.43). As a result, the present phosphors may serve as the potential emitting element for generating white light in combination with a complementary blue phosphor.

Conclusions

To sum up, we have prepared a family of cyclometalated Ir(III) complexes with novel diphenyl(1-naphthyl)phosphine ancillary isomerization, via the sequential transformation from simple phosphine addition at the Ir(III) metal center and cyclometalation at the coordinated phosphine. For the present molecular architecture, it is essential to employ the aromatic cyclometalates with at least one fluorine substituent, which plays a pivotal role in strengthening the metal−ligand bonding and provides the much desired chemical and thermal robustness during their syntheses. All complexes exhibited high emission efficiencies in solution state; particularly, the quantum yield of **4b** is near unity in the red. Computational results suggest that, upon variation of the C^N cyclometalates from quinazolinyl, isoquinolinyl, and, finally, to pyridyl fragment, the LUMO orbitals are suddenly shifted from the cyclometalated nitrogen heterocycles to the 1-naphthyl group of the cyclometalated phosphine for the isomers **a**, **b** and to **c**. Accordingly, the excited-state characteristics are switching from (**a**) MLCT + LLCT to (**b**) MLCT + ILCT on C^N chelates and, finally to (**c**) MLCT + ILCT on the cyclometalating phosphine, which concomitantly alter the intrinsic photophysical properties (see Table of Content illustration). This result rules out the possibility of using such diphenyl(1-naphthyl)phosphine ancillary in stabilizing the shorter wavelength, green or blue-emitting metal phosphors. Nevertheless, the electroluminescence of **4a** and **4b** obtained with the as-fabricated OLED devices is highly efficient. These findings suggest that the related orange and or red-emitting Ir(III) complexes with strategic and rational design could play an important role for the future development of triplet OLED emitters.

Acknowledgment. This work was supported by the National Science Council of Taiwan. We are also grateful to the National Center for High-performance Computing for computer time and facilities.

Supporting Information Available: Selected spectral data of cyclometalate ligands, synthesis of chloride-bridged Ir(III) dimer, cyclic voltammogram, frontier orbitals and orbital energies involved in the lower-lying transition for all complexes **3** and **4**, X-ray crystallographic data file (CIF) of the studied complexes **1a**, **2a**, **3c**, **4a**, and **4c**. This material is available free of charge via the Internet at http://pubs.acs.org.